Cronfa - Swansea University Open Access Repository

_____

This is an author produced version of a paper published in:
Accounts of Chemical Research

_____

Cronfa URL for this paper:

_____

Paper:

_____
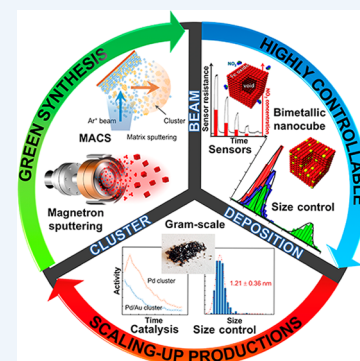
ACCOUNTS
of chemical research

pubs.acs.org/accounts

Synthesis without Solvents: The Cluster (Nanoparticle) Beam Route to Catalysts and Sensors

Richard E. Palmer,* Rongsheng Cai, and Jerome Vernieres

College of Engineering, Swansea University, Bay Campus, Fabian Way, Swansea SA1 8EN, United Kingdom

CONSPECTUS: It is hard to predict the future of science. For example, when C_{60} and its structure were identified from the mass spectra of gas phase carbon clusters, few could have predicted the era of carbon nanotechnology which the discovery introduced. The solubilization and functionalization of C_{60}, the identification and then synthesis of carbon nanotubes, and the generation and physics of graphene have made a scale of impact on the international R&D (and to some extent industrial) landscape which could not have been foreseen. Technology emerged from a search for molecules of astrochemical interest in the interstellar gas. This little sketch provides the authors with the confidence to present here a status report on progress toward another radical future—the synthesis of nanoparticles (typically metals) on an industrial scale without solvents and consequently effluents, without salts and their sometimes accompanying toxicity, with minimal prospects for unwanted nanoparticle escape into the environment, with a high degree of precision in the control of the size, shape and composition of the nanoparticles produced and with applications from catalysts and sensors to photonics, electronics and theranostics. In fact, our story begins in exactly the same place as the origin of the nanocarbon era—the generation and mass selection of free atomic clusters in a vacuum chamber. The steps along the path so far include deposition of such beams of clusters onto surfaces in vacuum, elucidation of the key elements of the cluster−surface interaction, and demonstrations of the potential applications of deposited clusters. The principal present challenges, formidable but solvable, are the necessary scale-up of cluster beam deposition from the nanogram to the gram scale and beyond, and the processing and integration of the nanoclusters into appropriate functional architectures, such as powders for heterogeneous catalysis, i.e., the formulation engineering problem. The research which is addressing these challenges is illustrated in this Account by examples of cluster production (on the traditional nanogram scale), emphasizing self-selection of size, controlled generation of nonspherical shapes, and nonspherical binary nanoparticles; by the scale-up of cluster beam production by orders of magnitude with the magnetron sputtering, gas condensation cluster source, and especially the Matrix Assembly Cluster Source (MACS); and by promising demonstrations of deposited clusters in gas sensing and in heterogeneous catalysis (this on the gram scale) in relevant environments (both liquid and vapor phases). The impact on manufacturing engineering of the new paradigm described here is undoubtedly radical; the prospects for economic success are, as usual, full of uncertainties. Let the readers form their own judgements.

1. INTRODUCTION

By definition, nanoparticles (NPs) or nanomaterials are small objects in the range of 1−100 nm,[1] usually defined as an agglomeration of atoms or molecules which exhibit a wide range of size-dependent properties.[2] NPs with tailored morphologies and chemical composition have attracted great attention due to their unique properties. They can lead to highly advantageous characteristics in applications such as heterogeneous catalysis,[3,4] plasmonics,[5,6] or biomedicine.[7,8] The fabrication methods of nanomaterials are classified into two categories: (i) top-down methods and (ii) bottom-up methods. The latter is of interest in this Account and can be divided into two approaches, the chemical and physical methods. The chemical approaches are the most widely used, as they offer a high control over the size, shape and chemical composition.[9−11] However, the chemical approaches often involve chemical agents associated with environmental toxicity. Thus, it is highly desirable to find novel *green* synthesis approaches for NP production, either by using environmental-friendly solvents methods[12] or solvent-free synthesis such as gas-phase methods.

2. CLUSTER BEAM DEPOSITION (CBD) METHOD

Despite the technical demands of gas-phase synthetic methods, the CBD method has emerged as one of the most promising techniques for producing supported NP assemblies. Typically, gas-phase synthesis relies on homogeneous nucleation of a supersaturated vapor, for example metal atoms within a low-pressure rare gas environment, followed by particle growth via condensation and coalescence.[13] Among the variety of CBD methods available to date, the magnetron-sputtering, inert-gas condensation method[14] has emerged as one of the most versatile as it allows control of the growth process by varying the experimental parameters such as the magnetron power, the
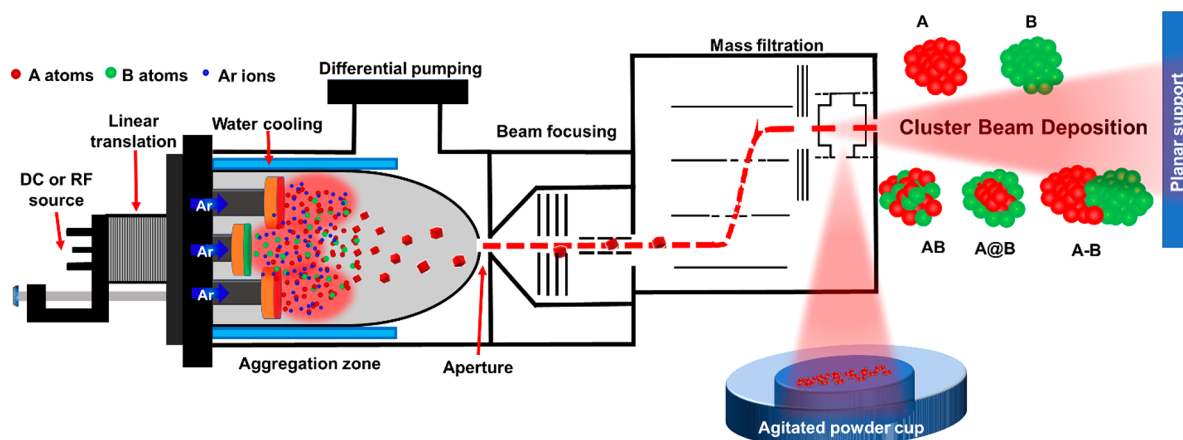
Figure 1. Schematic illustration of magnetron sputtering nanoparticle deposition setup showing the aggregation zone where the nucleation and growth occur. Nanoparticles fly toward the deposition chamber by differential pressure forming a cluster beam of monatomic species A and B, or binary nanoparticles such as mixed structure (AB), core−shell structure (A@B), and Janus structure (A-B). The nanoparticle beam is deposited onto planar supports or powders after passing through a focusing stage and mass filtration unit for size-selection.

inert-gas pressure and the length of the aggregation zone (Figure 1).

In recent years, a new generation of CBD sources has emerged[15,16] which enables not only the synthesis of single-component NPs, but also multicomponent NPs via the use of two or more independent target materials (Figure 1). The capability to use multiple independent targets opens new avenues for the design and preparation of multimetallic NPs with control of their morphology and composition, in a single synthetic protocol. For binary NPs, three main types of NP morphologies (Figure 1) have been reported, which differ in the atomic arrangements of the two elements (A and B) within the same NP: (i) NP alloys (AB or BA), which can be either random[17] or ordered;[18,19] (ii) core@shell NPs (A@B),[20] which consist of one type of atoms (B) surrounding a core of another type of atoms (A); and (iii) the commonly named Janus NPs (A-B), which consist of two parts of different elements sharing a common interface.[21]

Discussion of these morphologies has invoked thermodynamic considerations which determine the driving forces and stability of the different NPs.[22,23] However, a more in-depth understanding of the underlying mechanisms of NP growth has also highlighted kinetic effects, for example, to explain the formation mechanism of cuboid shapes in gas-phase synthesis.[24] Among these different morphologies, CBD methods also offer the ability to size-control the NPs by postgrowth separation phase (Figure 1), such as time-of-flight[25,26] (TOF) or quadrupole mass-filtration.[27] However, size separation challenges the utilization of gas-phase condensation techniques for large scale production of nanoparticles.[25] In this Account, we highlight methods that focus on accurate determination of nanoparticle sizes during the growth, instead of producing a wide size-dispersion first followed by mass-filtration afterward. In particular, we consider the potential of nanoparticle self-arrangement during gas-phase growth, and a new class of CBD source, the Matrix Assembly Cluster Source (MACS) that promises a breakthrough in large-scale production of clusters.

3. STRUCTURE-CONTROL IN CLUSTER BEAM DEPOSITION

### 3.1. Size-Control during Formation in the Gas-Phase

The control of the particle size remains a primary aim in the preparation of metal NPs, whether by physical or chemical means. In CBD, this control is commonly ensured by size-selection after NP growth, which limits the obtainable material yield considerably. Thus, it is highly desirable to find new routes to size-selection during the formation process.

A novel methodology to ensure simultaneous size and shape control during cluster formation was recently reported; this work introduced the ferromagnetic (Fe) target thickness as a decisive experimental parameter.[28] Previous studies showed the limiting effects of screening by the high-permeability of a magnetic target, but this factor can also be exploited as a tool to control NP growth. On the grounds that nucleation happens within a short distance of the sputtering target, this effect can tune the NP size. The magnetic target thickness was adjusted from 0.3 to 1 mm, with the effects illustrated in Figure 2a. A switch from bimodal size distribution to a well-defined single peak in the mass spectrum is observed. The work revealed a close correlation between the width of the target erosion profile (Figure 2b) and the shape of the cluster size-distribution, mainly its width (standard deviation). This is consistent with modification of the electron trap region close to the surface by the magnetic screening induced by the target. In addition, to validate the approach regarding the accurate control of the size during formation, similar experiments were performed with and without the quadrupole mass filter. Interestingly, there was no gain in standard deviation using mass filtration, but a significant decrease of the material yield compared to experiment without mass filtration was observed, as shown in Figure 2c.

3.2. Shape-Control of Iron Nanoparticles

Besides the size-control ability shown previously using the gas-phase method, the morphology of NPs, in particular the shape, is of importance in some aspects of nanotechnology.[29,30] A striking example of NP shape control in CBD is the ability to switch readily the shape of Fe NPs from cubic (Figure 3a) to quasi-spherical (Figure 3b) by only adjusting the dc magnetron power of the sputtering source.[24] The magnetron power
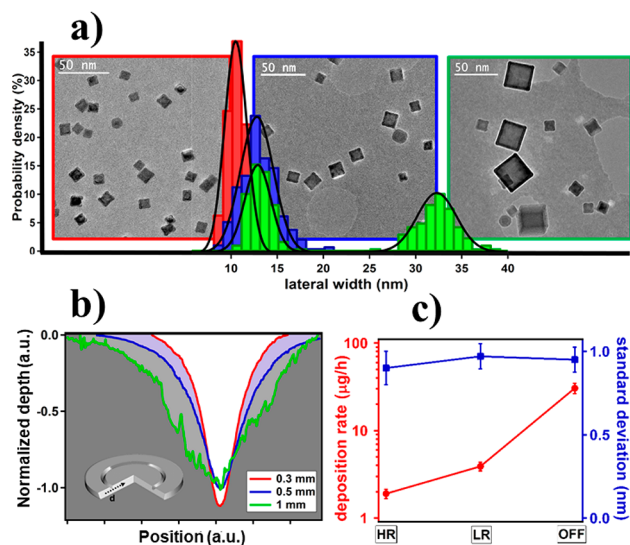
Figure 2. (a) Size dependence of Fe nanoparticles as a function of the thickness of the magnetic target (0.3 mm in red; 0.5 mm in blue; 1 mm in green). Distinct transition from bimodal to single size distribution was observed. (b) Clear correlation between the standard deviation of the size distribution and the corresponding racetrack profile was revealed via profilometry measurements. (c) Relationship between the deposition rate and standard deviation of Fe nanocubes for different mass filter settings. The labels "LR", "HR", and "OFF" represent low-resolution, high-resolution, and without mass filtration, respectively. Reproduced with permission from ref 28. Copyright 2017 John Wiley and Sons.

dictates the NP shape, by providing a way to control the number of metal atoms ejected from the target materials (Fe atom density) as well as the thermal environment by increasing the probability of metal–metal atom collisions instead of metal–Ar collisions.

For comparison, in chemical synthesis methods, the well-known ability of surfactants to bind preferentially to specific facets allows different facet growth rates, thus providing a means of tuning the NP shapes.[31] But what can explain the control of the cuboid NP growth using physical methods? One way to scrutinize subtle kinetics effects on the growth, such as the competition between surface diffusion rates on specific facets with the rates of atomic deposition, is to employ a combination of molecular dynamics and kinetic Monte Carlo simulations. As shown in Figure 3c, the competition between a layer-by-layer growth mode (Frank-van-der-Merwe-like (FM)) on the {100} facet and an island growth mode (Volmer–Weber-like (VW)) on the {110} facet is the driving force for growth of cubic rather than near-spherical shapes. This study has revealed the possibility to stabilize cubic shape which is energetically unfavorable at thermodynamic equilibrium using gas-phase methods.

3.3. Bimetallic Iron-Based Nanocubes

While improved control of size and shape of monometallic NPs is a significant development, it is insufficient to fulfill the demand for optimized multifunctional nanomaterials. Our deposition approach has been recently extended to bimetallic NPs using a co-sputtering process with nonmagnetic dopants,[28,32] while keeping uniformity in size, shape, and crystallinity.

As a demonstration of binary nanoparticle control, Figure 4 shows a study of the Fe–Pd system using three independent
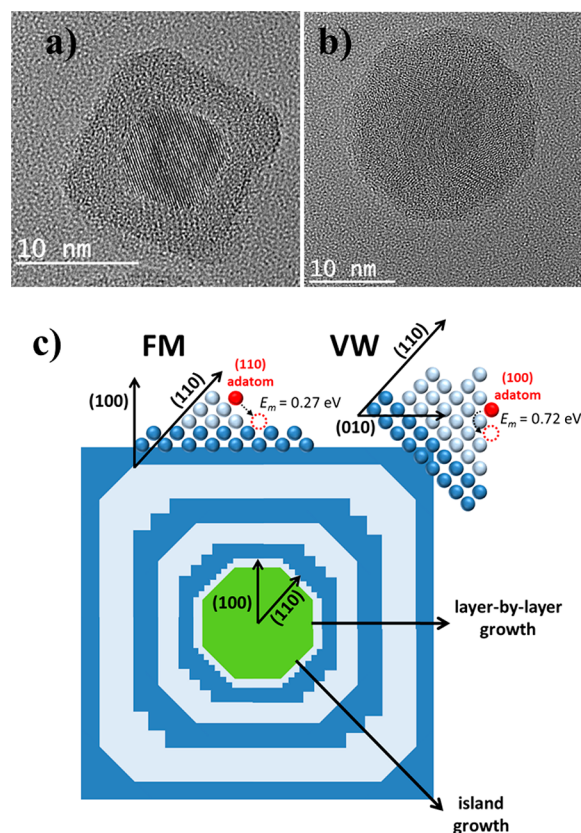

Figure 3. Clear evidence of shape control from cuboid morphology (a) to spherical morphology (b) for Fe nanoparticles is shown by high-resolution TEM images. A core–shell structure can be observed after exposure to air. (c) Schematic of an initially faceted, truncated rhombic dodecahedron nanoparticle. Two competing mechanisms, the atomic deposition and surface diffusion, are responsible for the formation of the cubic shape, . Temporal evolution is represented by the light and dark blue colors of the extra-deposited adatom layers. Nanoislands of {110} and {100} sides are grown on {100} and {110} facets, respectively, as shown in the zoomed areas. Different growth modes are distinguished: {110} facets grow via VW-like mechanism (island growth) and {100} facets via a FM-like mechanism (layer-by-layer growth), leading to two different growth rates. Reproduced with permission from ref 24. Copyright 2016 American Chemical Society.

targets simultaneously. Well-defined FePd nanocubes are obtained with a narrow size distribution, as shown in Figure 4a. A core–shell morphology with a highly crystalline core is revealed after air exposure, as shown in the inset to Figure 4a, in high-angle annular dark field image (HAADF) in scanning TEM (STEM) mode. Furthermore, spatially localized electron energy loss-spectra (EELS) from the STEM clearly distinguish the presence of both Fe and Pd within the core while only Fe oxide exists in the shell (Figure 4b). Multiple characterization techniques indicate that the FePd core has a random alloy arrangement with an estimated chemical composition of 10–15% of Pd. All these results show the highly controllable features of these techniques, such as the capacity of noble metal (Pd, Au) doping to form bimetallic nanoparticles while keeping the highly uniform size and shape seen previously.

4. SCALE-UP OF THE CLUSTER PRODUCTION RATE

The successful control of size, shape and composition of the clusters formed by synthesis in the gas-phase has made the cluster beam technique a powerful tool to investigate the
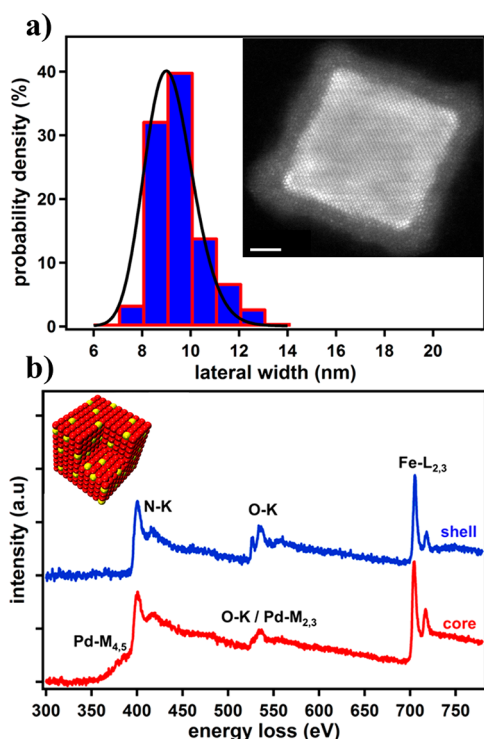
Figure 4. Synthesis of bimetallic FePd nanocubes using CBD. (a) Size probability density showing a narrow distribution center around 9 nm. Corresponding HAADF-STEM image of a representative FePd nanocube showing a crystalline core and oxide shell (inset in (a), scale bar 2 nm). (b) Electron energy loss-spectroscopy (EELS) at the core and shell position confirmed the bimetallic nature within the core and the formation of an Fe oxide shell. Reproduced with permission from ref 32. Copyright 2017 Royal Society of Chemistry.

fundamental properties of clusters on surfaces and has also stimulated studies of size-dependent catalytic activity on the 1 cm^2 surface area scale, i.e., in the domain of surface science. However, its application to making catalysts at the standard chemistry laboratory research scale, let alone industrial levels, is hampered by the low production rates. For example, a conventional cluster beam source can typically produce a size-selected cluster beam current of about ~0.1−1 nA (equivalent to 0.05−0.5 μg Au$_{100}$ clusters/h). Thus, a prohibitive time is needed even to produce 1 g of catalyst loaded with 10 mg of clusters (1 wt % loading) for standard catalytic R&D measurements. Therefore, very significant scale-up of the cluster production rate is a crucial challenge if the cluster beam technique is to contribute at this level. Thus, reported developments in high flux cluster beam instruments are of particular interest. However, we should also be aware that the current studies have not yet been able to achieve the size/shape/composition control and high cluster deposition rate at the same time. Hopefully, in the future, both features could be obtained together with the help of more advanced cluster beam techniques. Here we highlight two innovations of high flux cluster beam instruments.

4.1. Magnetron-Sputtering Gas Condensation Cluster Source

A scale-up of 2 orders of magnitude has been achieved with a traditional magnetron sputtering, gas condensation cluster source,[33,34] simply by extraction of the cluster beam before the mass spectrometer, which is only used for monitoring the

cluster size distribution; the scheme is shown in Figure 5a. The instrument consists of four sections: magnetron sputtering, gas
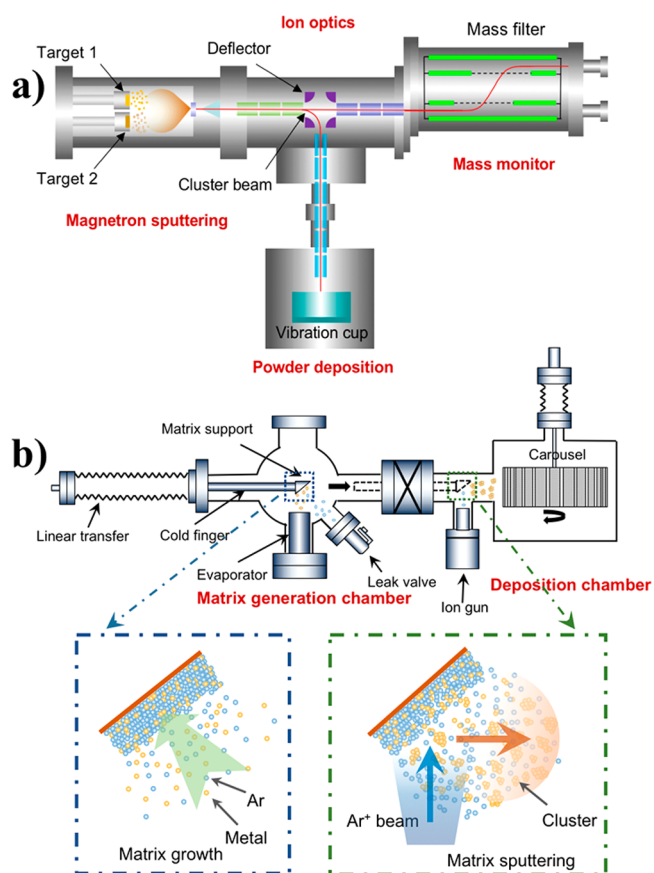
Figure 5. Schematic diagrams of two different cluster sources, which are used to scale up the cluster production rate. (a) Dual-magnetron sputtering, gas condensation cluster source, in which the positively charged clusters are controlled by an "octosphere" deflector, either for deposition onto agitated powders or for mass monitoring. (b) A MACS, in which a solid matrix is first prepared on a cryogenically cooled matrix support by co-condensing inert gas atoms and atoms of target material. An Ar ion beam is then employed to sputter the matrix, causing clusters to nucleate, ripen, and eventually be impacted out. Reproduced with permission from ref 17, Copyright 2018 John Wiley and Sons; ref 36, Copyright 2017 American Institute of Physics.

condensation chamber; ion optics chamber; mass filter chamber; and cluster deposition chamber. The sputtering chamber includes two magnetrons mounted in parallel, which allow for tuning of the composition of binary clusters. An electrostatic "octosphere" deflector allows the ionized cluster beam to fly directly into the mass filter to measure the size distribution or deflects it down by 90° toward the deposition chamber. Here a future innovation is introduced. Powder supports loaded into a stainless-steel cup are mechanically agitated close to the beam deposition to maximize exposure of powder to the incoming cluster beam. The typical cluster beam deposition current is around 20−50 nA, which enables the deposition of 0.1 wt % Au$_{300}$ clusters onto 1 g of powder in 10 h. An example of early catalytic studies with the cluster-decorated powders produced is discussed in section 5.2.

4.2. Matrix Assembly Cluster Source (MACS)

A new type of nanoparticle beam source, MACS,[35] has recently been invented and demonstrated in an attempt to reach cluster

beam intensities sufficient to 1 g of catalyst in 1 h. The principle of this new system is different from the traditional method of condensing hot atoms in a cold gas. Instead, the MACS is the impact of an ion beam (e.g., Ar^+) upon a condensed matrix of rare gas atoms impregnated with atoms of the desired material. The impact of an ion initiates a cascade of collisions inside the matrix, causing clusters to nucleate and/or ripen. A cluster can be ejected from the matrix by the same (or subsequent) ion beam impact. Figure 5b shows a schematic diagram of a prototype MACS.[36] The solid matrix is prepared on a cryogenically cooled (~10 K) matrix support by condensation of rare gas atoms while the cluster material is evaporated at the same time. Once the matrix is prepared, it is then moved to the second chamber in this system for sputtering. A carousel holding up to 21 glass slides is designed to collect the clusters sputtered out of the matrix. The cluster flux is linearly proportional to the incident ion beam current (~1 cluster is emitted per 100 Ar^+ impacts),[33] so further scale-up can be achieved by employing a more powerful ion source (here 100 μA). Indeed, a scale up of 5 orders of magnitude has been achieved, from 100 nanograms of clusters per hour to 10 mg per hour with an Ar ion beam of ~1 mA current. In addition, compared with a traditional gas condensation source in which much of the material (>90%) is deposited on the walls of the condensation chamber, the MACS offers in principle 100% utilization, since all the material loaded into the matrix can be sputtered out and collected or recovered from the matrix support plate after use.

In the emerging understanding of how clusters are formed in the MACS matrix, molecular dynamics simulations have played a valuable role in illustrating the ion bombardment of three Ar matrices with Ag content of 5%, 10%, and 20%.[37] It was found that clusters in the matrix ripen via multiple ion impacts. Figure 6a shows the average size of Ag clusters formed in the matrix as a function of the number of impact Ar ions. For all three cases, the Ag clusters grow with successive collision cascades, especially for the matrix with 20% Ag loading. But how do such clusters escape from the matrix? The emission process was simulated for a model system containing an individual Ag cluster embedded in an Ar matrix around 1 nm below the surface (Figure 6b). The simulations showed that a direct collision between the incident Ar atom and the embedded Ag cluster. The cluster temperature rise was sufficient to boil the Ar layer around the cluster surface. Moreover, the momentum transferred from incident Ar atom to cluster accelerated the cluster toward the bulk of the matrix. The recoil due to the compression of the matrix was sufficient to drive the cluster out of the matrix.

5. APPLICATIONS OF CLUSTER BEAM DEPOSITED CLUETERS IN SENSING AND CATALYSIS
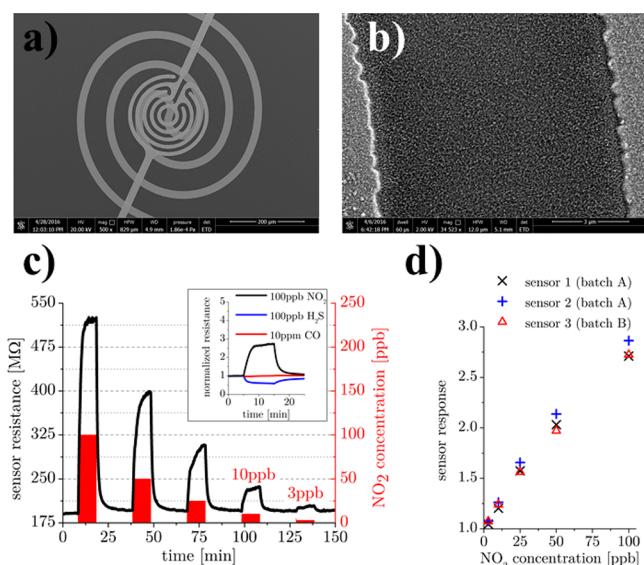
5.1. Gas Sensing: NO_2 Detection

Chemoresistive metal oxide gas sensors[38,39] have potential applications in environmental monitoring and biomedical diagnostic. For examples, nitrogen oxides (NO_x, mainly consisting of NO and NO_2) are industrially and biologically important gas species, which can be potential markers of pathologies such as asthma.[40,41] In the field of breath diagnosis, the need to fabricate highly reproducible, stable, and highly sensitive NO_2 sensors with an accuracy of 1 ppb in a range of 1−500 ppb remains a significant challenge. The optimization of semiconducting metal oxide materials in terms of
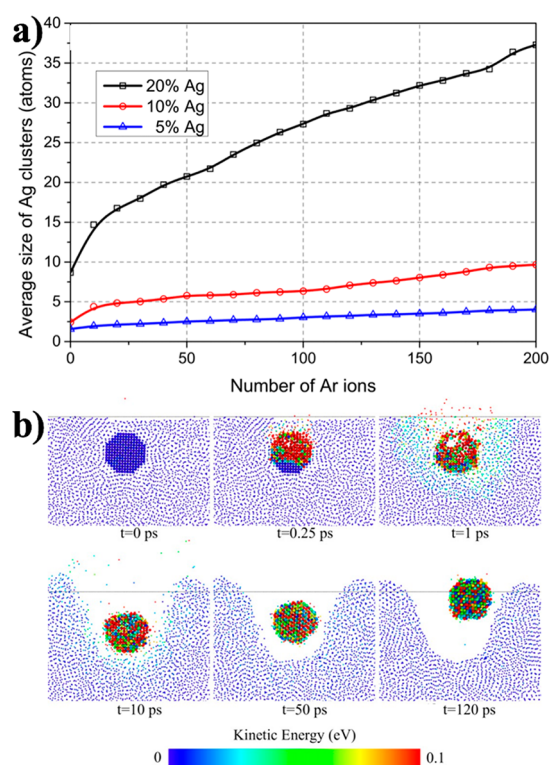
Figure 6. Molecular dynamics simulations of the cluster formation mechanism in MACS. (a) Evolution of the average size of Ag clusters formed in the Ar matrix as a function of the number of impacted Ar ions. (b) Series of simulation snapshots of a two-dimensional sliced cross-sectional model system. An individual Ag cluster is embedded in an Ar matrix about 1 nm below the surface. Color bar shows the kinetic energy for metal atoms from 0 to 0.1 eV. Reproduced with permission from ref 37. Copyright 2017 American Physical Society.

selectivity[42] and low operation temperature[43] using catalytic NPs has been extensively investigated. However, the use of expensive metals (Pd, Pt, Au, etc.) remains a limitation, as well as the lack of information on the interplay between their atomic-scale structure and their influence on the sensing properties. The development of scalable nanomaterials preparation methods may play a role in addressing this problem. CBD is well suited for CMOS-compatible sensor production because it allows single-step NP deposition at room temperature under high vacuum conditions without the presence of precursors and surfactants.

A sensor fabricated with the Fe NP production technology described in section 3.1 is shown in Figure 7. The clusters were deposited onto an electrode array (Figure 7a) and produced a percolating film of Fe nanocubes (Figure 7b). The circular-shaped metal electrodes were fabricated on a micro hot plate[44] support by lithographic techniques, which allows local heating during sensor operation. Gas sensing experiments were performed in a commercial probe station, measuring the electrical resistance changes during exposure. Figure 7c shows the resistance change of the Fe nanocube film in dry synthetic air during exposure to pulses of NO_2 (concentration range 3−100 ppb) at temperature of 200 °C. A sensitivity down to the 3-ppb level was established, which meets the specification for asthma detection. This approach shows better performance than conventional Fe-based sensors,[45] as well as competing favorably with other nanomaterial such as 1D metal oxides[46] or 2D materials.[47] Results with other toxic gases are shown in the

Figure 7. Chemoresistive gas sensing for NO_2 detection at a very low-level. Scanning electron microscopy images of (a) the microhot plate device and (b) the Fe nanocube layer between the sensing electrodes. (c) Resistance change of the percolating Fe nanocube film during exposure to ppb-level of NO_2 at the temperature of 200 °C. Inset: Selectivity measurements of the gas sensor showing the normalized resistance change during exposure to 100 ppb of NO_2, 100 ppb of H_2S, and 10 ppm of CO. (d) Sensor response R_{NO_2}/R_{air} for two different sensor batches showing highly reproducibility signals over all the NO_2 concentration range with a linear behavior. Reproduced with permission from ref 28. Copyright 2017 John Wiley and Sons.

inset of Figure 7c. The nonzero response found for H_2S gas compared with CO is well described by an n-type metal oxide semiconductor model. H_2S can be easily distinguished from NO_2 by the sign of the resistance change. The reproducibility of the sensors across two different batches is shown in Figure 7d. The analysis of the sensing mechanism is something of a puzzle in the literature. Indeed, with elevated temperatures and oxidizing/reducing gas atmospheres, a severe impact on the nanoscale morphology of the sensing elements can be anticipated. In this case, environmental-TEM revealed the formation of voids at the centers of the NPs under operational condition,[28,32] which gives a possibility to understand the sensing performance and stability after operation. The excellent sensing properties due to specific NP morphologies combined with the inherent advantages of NP gas-phase synthesis make the CBD approach a highly promising candidate for future large-scale production of miniaturized, high-performance gas sensor devices integrated with standard microelectronic components.

5.2. Catalysis Applications

Physically produced metal clusters deposited onto powder supports with tunable interaction represents a new paradigm in making heterogeneous catalysts for different applications, from fine chemistry to petrochemistry, from electrocatalysis to photocatalysis. Scale-up of the rate of cluster beam deposition, especially at the gram scale, opens the way to explore catalytic behaviors under realistic reaction conditions. Here we review two recent examples of cluster catalysis, one in the liquid phase and one in the vapor phase, at the test tube or beaker rather than surface science scale.

5.2.1. 4-Nitrophenol Reduction in Solution. The reduction of nitrophenol by sodium borohydride ($NaBH_4$) is an attractive model reaction to evaluate cluster catalytic activities in solution, since the reagents and products can be measured precisely by real-time spectroscopy. In this study, Au/Cu binary clusters (spherical shape; diameter in the range of 3−5 nm) with three different compositions (termed Au-rich, Au/Cu-balanced and Cu-rich), were deposited onto MgO powder supports by the dual magnetron sputtering gas condensation cluster beam source discussed in Figure 5a.[17] Cluster composition measurements indicated a strong relationship between the Au/Cu atomic ratio and the power applied to the two sputtering targets. Figure 8a and b shows a HAADF-
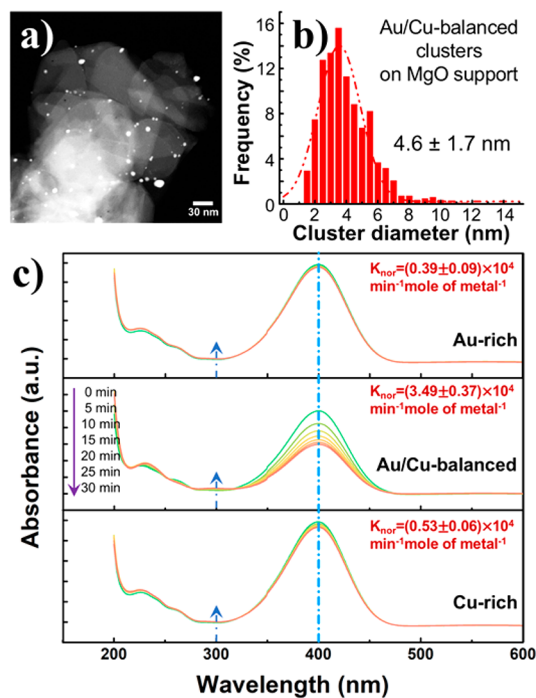
Figure 8. Catalytic performance of Au/Cu clusters deposited on MgO powder supports in reduction of 4-nitrophenol. (a) Typical HAADF-STEM image of Au/Cu-balanced cluster catalyst produced by a dual-magnetron sputtering gas condensation cluster source. (b) Diameter distribution histogram of the Au/Cu-balanced clusters on MgO powder support. (c) UV−vis absorbance spectra of the 4-nitrophenol reduction catalyzed by Au/Cu cluster catalysts (5 min intervals). The intensity of the peak at 400 nm represents the concentration of 4-nitrophenol in the solution, which indicates Au/Cu-balanced cluster catalyst is more active than Au-rich and Cu-rich cluster catalysts. Intrinsic reaction rate constant, K_{nor}, was used to compare the cluster activity, which is obtained by normalizing the apparent reaction rate constant by the total mole of metals. Reproduced with permission from ref 17. Copyright 2018 John Wiley and Sons.

STEM image and corresponding diameter distribution for the Au/Cu-balanced cluster catalyst. The measured average size on the MgO support (4.6 nm) was larger than the value estimated from the mass spectra (2.4 nm for a spherical shape), indicating that a degree of surface aggregation happens when the clusters landed on the powders. The Au/Cu catalysts produced were directly used to catalyze the reduction of 4-nitrophenol by $NaBH_4$ in solution. Figure 8c shows the evolution of the UV−vis absorbance spectra of the reaction solution after adding 30 mg Au/Cu cluster catalysts. For the Au/Cu-balanced cluster catalyst, the intensity of the peak at

400 nm, which indicates the concentration of 4-nitrophenol in the solution, decreases quickly with the reaction time. For the Au-rich and Cu-rich cluster catalysts, the peak intensity drops much more slowly, suggesting the Au/Cu-balanced cluster catalyst is more active than the Au-rich and Cu-rich cluster catalysts. Since the cluster loading for the different compositions was not identical, their activities are best compared through the normalized reaction rate constant, K_{nor} ($\text{min}^{-1} \cdot \text{mol metal}^{-1}$). For the Au/Cu-balanced cluster, the K_{nor} is 8.9 and 6.6 times that of Au-rich and Cu-rich clusters, respectively, which indicates that the Au/Cu-balanced cluster is much more active. DFT calculations on the binding energies of model cluster-reagent and cluster-product systems suggested that binding of the reagent molecules to an adjacent pair of Au and Cu atoms at the cluster surface optimized the relative energies for regent adsorption and product desorption, which could account for the enhanced catalytic activity.[17] This work shows an insight into design of bimetallic clusters at the atomic scale for highly active catalysts.

5.2.2. Selective Hydrogenation of 1-Pentyne. The selective hydrogenation of 1-pentyne to 1-pentene in the vapor phase is an important reaction, as it produces a high purity alkene steam which is widely used in the petrochemical industry.[48] Pd and Pd/Au clusters (spherical shape; diameter in the range of 1−2 nm) deposited with the MACS onto carbon tapes were used to catalyze this reaction and compared with a Pd reference sample prepared by impregnation. A dicing technique[49] was adopted to transform carbon tapes decorated by deposited clusters into catalyst powders, as shown in Figure 9a. The carbon tape supports were first mechanically diced to generate grooves on the surface. Then the diced supports were loaded onto the carousel and presputtered by an Ar ion beam; the point defects formed thus provide anchor sites for clusters on the surface to reduce aggregation. After cluster deposition, the topmost layer of the supports was scratched off to obtain the catalyst powders. Figure 9b and c shows a HAADF-STEM image and corresponding diameter distribution for the Pd cluster catalyst. Dense Pd clusters were observed on carbon flakes with an average diameter of 1.21 ± 0.36 nm. The cluster catalysts produced were directly used to catalyze the 1-pentyne hydrogenation reaction. The plots in Figure 9d compare the catalytic activity of the Pd cluster catalyst with the Pd reference sample in terms of activity per metal atom. The Pd cluster catalyst was found to be more active than the reference sample (average particle diameter 2.38 nm), consistent with the smaller particle size obtained with the MACS; thus, the number of active surface sites per unit weight of metals is increased. The Pd (1.21 ± 0.36 nm) and Pd/Au clusters (1.31 ± 0.41 nm) had the similar diameters, so the effect of composition on the catalytic activity could be explored. The product yields per surface atoms are shown in Figure 9e. It can be seen that the surface atoms on the binary nanoalloys exhibit a similar catalytic activity to those of the pure Pd clusters. One reasonable explanation is that oxidation drives the Pd atoms in the Pd/Au clusters to the surface when they are stored in air. Although a synergetic effect is not observed in the Pd/Au binary clusters, this study suggests a route to decrease the catalyst cost by design of core−shell bimetallic systems with a base metal at the core.

6. CONCLUSION

Cluster beam deposition provides a means to synthesize and deposit atomic clusters in vacuum with precise control of the
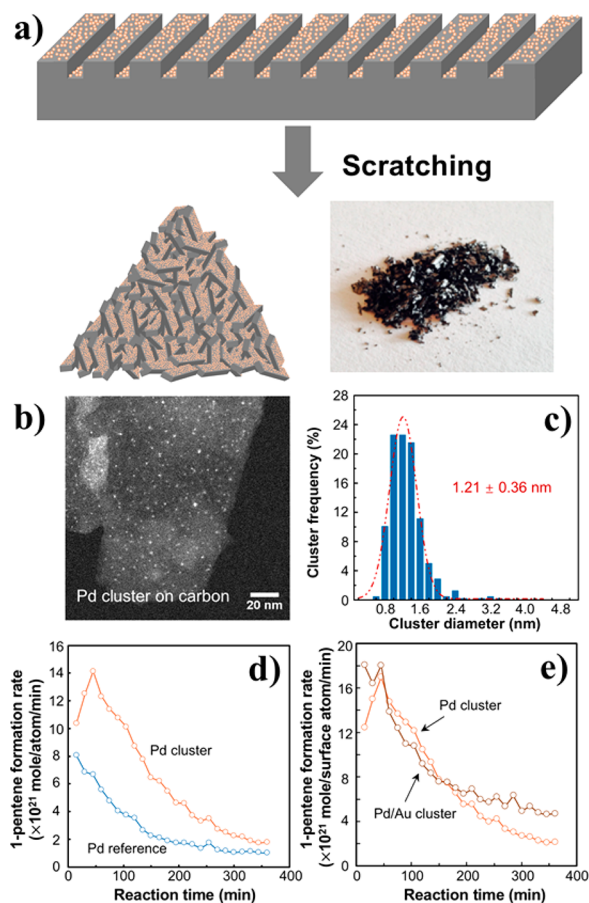
Figure 9. Selective 1-pentyne hydrogenation catalyzed by carbon supported Pd and Pd/Au clusters produced by MACS and a Pd reference sample made by impregnation. (a) Schematic diagram of the dicing technique which is used to transform cluster decorated carbon tapes to practical catalyst powders. (b) Representative HAADF-STEM image of the Pd cluster catalyst on carbon flakes and (c) the corresponding cluster diameter distribution. (d,e) Comparison of the cluster activity as a function of reaction time at a fixed temperature of 220 °C. (d) Plots of 1-pentene formation rate as a basis of per atom for Pd cluster catalyst and Pd reference sample. (e) Plots of 1-pentene formation rate as a basis of per surface atom for Pd and Pd/Au cluster catalyst. Reproduced with permission from ref 50. Copyright 2018 University of Birmingham.

size, shape, and composition without need for solvents, effluents, or salts. The deposition of clusters onto chosen supports, whether planar or powder, allows for the fabrication of functional systems including catalysts and sensors. In this Account, recent progress in the morphology control of clusters produced with a magnetron-sputtering, gas condensation cluster source has been illustrated through the generation of quasi-spherical and cubic Fe clusters as well as Fe/Pd nanoparticles; the former exhibit promising performance in NO_2 detection. Current efforts to address the bottleneck of the cluster beam deposition rate have been highlighted. In particular, the Matrix Assembly Cluster Source (MACS), based on the ion beam sputtering of a metal loaded, cryogenically condensed solid matrix, can increase the deposition rate by 5 orders of magnitude compared with a standard size-selected cluster beam source. This scale-up makes it possible to explore powder-supported cluster catalysts, created at the gram scale, in liquid-phase and vapor-phase catalytic reactions. Sensors and catalysts are but

two of the potential applications which come into view via nanoparticle structure control and scale-up. Green manufacturing by cluster beam deposition may thus emerge as a new paradigm for the industrial synthesis of functional nanostructured materials. Only time will tell.

■ AUTHOR INFORMATION

Corresponding Author

*E-mail: R.E.Palmer@Swansea.ac.uk.

ORCID ⊙

Richard E. Palmer: 0000-0001-8728-8083

Author Contributions

The authors contributed equally to this work.

Notes

The authors declare no competing financial interest.

Biographies

Richard E. Palmer is Senior Research Fellow in the College of Engineering (Nanomaterials Lab) at Swansea University's new Bay Campus, Professor of Physics at Nanjing University, Editor-in-chief of Advances in Physics X (Taylor & Francis), Editor of Elsevier's book series "Frontiers of Nanoscience". Born in Swansea, he obtained his PhD at the Cavendish Laboratory, Cambridge, under the supervision of Roy Willis.

Rongsheng Cai is a Research Officer in the Nanomaterials Lab, College of Engineering, Swansea University. He obtained his M.S. degree in Materials Science from Qingdao University (2014) and undertook a PhD at the University of Birmingham (2014−2018). His research interests focus on transmission electron microscopy and catalytic properties of deposited metal clusters.

Jerome Vernieres, currently Research Officer at Swansea University, College of Engineering, received his PhD from the University of Toulouse, France under the guidance of Jean-François Bobo and completed his postdoctoral studies with Mukhles Sowwan at OIST, Japan. His research interest focuses on the design of multifunctional nanomaterials for sensing, biomedicine and catalysis.

■ ACKNOWLEDGMENTS

■ REFERENCES

(1) Kreyling, W. G.; Semmler-Behnke, M.; Chaudhry, Q. A complementary definition of nanomaterial. *Nano Today* **2010**, *5*, 165−168.

(2) Wells, D. M.; Rossi, G.; Ferrando, R.; Palmer, R. E. Metastability of the atomic structures of size-selected gold nanoparticles. *Nanoscale* **2015**, *7*, 6498−6503.

(3) Hunt, S. T.; Roman-Leshkov, Y. Principles ans Methods for the Rational Design of Core-Shell Nanoparticle Catalysts with Ultralow Noble Metal Loadings. *Acc. Chem. Res.* **2018**, *51*, 1054−1062.

(4) Blackmore, C. E.; Rees, N. V.; Palmer, R. E. Modular construction of size-selected multiple-core Pt-TiO2 nanoclusters for electro-catalysis. *Phys. Chem. Chem. Phys.* **2015**, *17*, 28005−28009.

(5) Wang, H.; Brandl, D. W.; Le, F.; Nordlander, P.; Halas, N. J. Nanorice: A Hybrid Plasmonic Nanostructure. *Nano Lett.* **2006**, *6*, 827−832.

(6) Park, J.-E.; Kim, S.; Son, J.; Lee, Y.; Nam, J.-M. Highly Controlled Synthesis and Super-Radiant Photoluminescence of Plasmonic Cube-in-Cube Nanoparticles. *Nano Lett.* **2016**, *16*, 7962−7967.

(7) Kim, S.-J.; Choi, S.-J.; Jang, J.-S.; Cho, H.-J.; Kim, I.-D. Innovative Nanosensor for Disease Diagnosis. *Acc. Chem. Res.* **2017**, *50*, 1587−1596.

(8) Rick, J.; Tsai, M.-C.; Hwang, B. J. Biosensors Incorporating Bimetallic Nanoparticles. *Nanomaterials* **2016**, *6*, 5.

(9) Peng, Z. A.; Peng, X. Nearly Monodisperse and Shape-Controlled CdSe Nanocrystals via Alternative Routes: Nucleation and Growth. *J. Am. Chem. Soc.* **2002**, *124*, 3343−3353.

(10) Habas, S. E.; Lee, H.; Radmilovic, V.; Somorjai, G. A.; Yang, P. Shaping binary metal nanocrystals through epitaxial seeded growth. *Nat. Mater.* **2007**, *6*, 692−697.

(11) Lacroix, L.-M.; Gatel, C.; Arenal, R.; Garcia, C.; Lachaize, S.; Blon, T.; Warot-Fonrose, B.; Snoeck, E.; Chaudret, B.; Viau, G. Tuning Complex Shapes in Platinum Nanoparticles: From Cubic Dentrites to Fivefold Stars. *Angew. Chem., Int. Ed.* **2012**, *51*, 4690−4694.

(12) Sharma, V. K.; Yngard, R. A.; Lin, Y. Silver nanoparticles: Green synthesis and their antimicrobial activities. *Adv. Colloid Interface Sci.* **2009**, *145*, 83−96.

(13) Swihart, M. T. Vapor-phase synthesis of nanoparticles. *Curr. Opin. Colloid Interface Sci.* **2003**, *8*, 127−133.

(14) Haberland, H.; Karrais, M.; Mall, M.; Thurner, Y. Thin films from energetic cluster impact: A feasibility study. *J. Vac. Sci. Technol., A* **1992**, *10*, 3266−3271.

(15) Martinez, L.; Diaz, M.; Roman, E.; Ruano, M.; Llamosa P., D.; Huttel, Y. Generation of nanoparticles with adjustable size and controlled stoichiometry: recent advances. *Langmuir* **2012**, *28*, 11241−11249.

(16) Benelmekki, M.; Bohra, M.; Kim, J. H.; Diaz, R. E.; Vernieres, J.; Grammatikopoulos, P.; Sowwan, M. A facile single-step synthesis of ternary multicore magneto-plasmonic nanoparticles. *Nanoscale* **2014**, *6*, 3532−3535.

(17) Cai, R.; Ellis, P. R.; Yin, J.; Liu, J.; Brown, C. M.; Griffin, R.; Chang, G.; Yang, D.; Ren, J.; Cooke, K.; Bishop, P. T.; Theis, W.; Palmer, R. E. Performance of preformed Au/Cu nanoclusters deposited on MgO powders in the catalytic reduction of 4-nitrophenol in solution. *Small* **2018**, *14*, 1703734.

(18) Mukherjee, P.; Manchanda, P.; Kumar, P.; Zhou, L.; Kramer, M. J.; Kashyap, A.; Skomski, R.; Sellmyer, D.; Shield, J. E. Size-induced chemical and magnetic ordering in individual Fe-Au nanoparticles. *ACS Nano* **2014**, *8*, 8113−8120.

(19) Vernieres, J.; Benelmekki, M.; Kim, J.-H.; Grammatikopoulos, P.; Bobo, J.-F.; Diaz, R. E.; Sowwan, M. Single-step gas phase synthesis of stable iron aluminide nanoparticles with soft magnetic properties. *APL Mater.* **2014**, *2*, 116105.

(20) Ghosh Chaudhuri, R.; Paria, S. Core/shell nanoparticles: classes, properties, synthesis mechanisms, characterization, and applications. *Chem. Rev.* **2012**, *112*, 2373−2433.

(21) Benelmekki, M.; Vernieres, J.; Kim, J.-H.; Diaz, R.-E.; Grammatikopoulos, P.; Sowwan, M. On the formation of ternary metallic-dielectric multicore-shell nanoparticles by inert-gas condensation method. *Mater. Chem. Phys.* **2015**, *151*, 275−281.

(22) Palomares-Baez, J. P.; Panizon, E.; Ferrando, R. Nanoscale effects on phase separation. *Nano Lett.* **2017**, *17*, 5394−5401.

(23) Rahm, J. M.; Erhart, P. Beyond magic numbers: atomic scale equilibrium nanoparticle shapes for any size. *Nano Lett.* **2017**, *17*, 5775−5781.

(24) Zhao, J.; Baibuz, E.; Vernieres, J.; Grammatikopoulos, P.; Jansson, V.; Nagel, M.; Steinhauer, S.; Sowwan, M.; Kuronen, A.; Nordlund, K.; Djurabekova, F. Formation mechanism of Fe nanocubes by magnetron sputtering inert gas condensation. *ACS Nano* **2016**, *10*, 4684−4694.

(25) Hernandez-Fernandez, P.; Masini, F.; McCarthy, D. N.; Strebel, C. E.; Friebel, D.; Deiana, D.; Malacrida, P.; Nierhoff, A.; Bodin, A.; Wise, A. M.; Nielsen, J. H.; Hansen, T. W.; Nilsson, A.; Stephens, I. E.; Chorkendorff, I. Mass-selected nanoparticles of PtxY as model catalysts for oxygen electroreduction. *Nat. Chem.* **2014**, *6*, 732−738.

(26) Plant, S. R.; Cao, L.; Palmer, R. E. Atomic structure control of size-selected gold nanoclusters during formation. *J. Am. Chem. Soc.* **2014**, *136*, 7559−7562.

(27) Ganeva, M.; Peter, T.; Bornholdt, S.; Kersten, H.; Strunskus, T.; Zaporojtchenko, V.; Faupel, F.; Hippler, R. Mass spectrometric investigations of nano-size cluster ions produced by high pressure magnetron sputtering. *Contrib. Plasma Phys.* **2012**, *52*, 881−889.

(28) Vernieres, J.; Steinhauer, S.; Zhao, J.; Chapelle, A.; Menini, P.; Dufour, N.; Diaz, R. E.; Nordlund, K.; Djurabekova, F.; Grammatikopoulos, P.; Sowwan, M. Gas phase synthesis of multifunctional Fe-based nanocubes. *Adv. Funct. Mater.* **2017**, *27*, 1605328.

(29) Narayanan, R.; El-Sayed, M. A. Catalysis with transition metal nanoparticles in colloidal solution: nanoparticle shape dependence and stability. *J. Phys. Chem. B* **2005**, *109*, 12663−12676.

(30) Lee, N.; Choi, Y.; Lee, Y.; Park, M.; Moon, W. K.; Choi, S. H.; Hyeon, T. Water-dispersible ferrimagnetic iron oxide nanocubes with extremely high r_2 relaxivity for highly sensitive in vivo MRI of tumors. *Nano Lett.* **2012**, *12*, 3127−3131.

(31) Liao, H.; Zherebetskyy, D.; Xin, H.; Czarnik, C.; Ercius, P.; Elmlund, H.; Pan, M.; Wang, L.; Zheng, H. Facet development during platinum nanocube growth. *Science* **2014**, *345*, 916−919.

(32) Steinhauer, S.; Vernieres, J.; Krainer, J.; Kock, A.; Grammatikopoulos, P.; Sowwan, M. In situ chemoresistive sensing in the environmental TEM: probing functional devices and their nanoscale morphology. *Nanoscale* **2017**, *9*, 7380−7384.

(33) Ellis, P. R.; Brown, C. M.; Bishop, P. T.; Yin, J.; Cooke, K.; Terry, W. D.; Liu, J.; Yin, F.; Palmer, R. E. The cluster beam route to model catalysts and beyond. *Faraday Discuss.* **2016**, *188*, 39−56.

(34) Escalera-Lopez, D.; Niu, Y.; Yin, J.; Cooke, K.; Rees, N. V.; Palmer, R. E. Enhancement of the hydrogen evolution reaction from Ni-MoS₂ hybrid nanoclusters. *ACS Catal.* **2016**, *6*, 6008−6017.

(35) Palmer, R. E.; Cao, L.; Yin, F. Note: Proof of principle of a new type of cluster beam source with potential for scale-up. *Rev. Sci. Instrum.* **2016**, *87*, 046103.

(36) Cai, R.; Jian, N.; Murphy, S.; Bauer, K.; Palmer, R. E. A new method to prepare colloids of size-controlled clusters from a matrix assembly cluster source. *APL Mater.* **2017**, *5*, 053405.

(37) Zhao, J.; Cao, L.; Palmer, R. E.; Nordlund, K.; Djurabekova, F. Formation and emission mechanisms of Ag nanoclusters in the Ar matrix assembly cluster source. *Phys. Rev. Mater.* **2017**, *1*, 066002.

(38) Ramgir, N.; Datta, N.; Kaur, M.; Kailasaganapathi, S.; Debnath, A. K.; Aswal, D. K.; Gupta, S. K. Metal oxide nanowires for chemiresistive gas sensors: Issues, challenges and prospects. *Colloids Surf., A* **2013**, *439*, 101−116.

(39) Steinhauer, S.; Singh, V.; Cassidy, C.; Gspan, C.; Grogger, W.; Sowwan, M.; Kock, A. Single CuO nanowires decorated with size-selected Pd nanoparticles for CO sensing in humid atmosphere. *Nanotechnology* **2015**, *26*, 175502.

(40) Ou, J. Z.; Ge, W.; Carey, B.; Daeneke, T.; Rotbart, A.; Shan, W.; Wang, Y.; Fu, Z.; Chrimes, A. F.; Wlodarski, W.; Russo, S. P.; Li, Y. X.; Kalantar-zadeh, K. Physisorption-based charge transfer in two-dimensional SnS₂ for selective and reversible NO₂ gas sensing. *ACS Nano* **2015**, *9*, 10313−10323.

(41) Macagnano, A.; Bearzotti, A.; De Cesare, F.; Zampetti, E. Sensing asthma with portable devices equipped with ultrasensitive sensors based on electrospun nanomaterials. *Electroanalysis* **2014**, *26*, 1419−1429.

(42) Baik, J. M.; Zielke, M.; Kim, M. H.; Turner, K. L.; Wodtke, A. M.; Moskovits, M. Tin-oxide-nanowire-based electronic nose using heterogeneous catalysis as functionalization strategy. *ACS Nano* **2010**, *4*, 3117.

(43) Zhang, J.; Liu, X.; Neri, G.; Pinna, N. Nanostructured Materials for Room-Temperature Gas Sensors. *Adv. Mater.* **2016**, *28*, 795.

(44) Steinhauer, S.; Chapelle, A.; Menini, P.; Sowwan, M. Local CuO nanowire growth on microhotplates: In situ electrical measurements and gas sensing application. *ACS Sensors* **2016**, *1*, 503−507.

(45) Navale, S. T.; Bandgar, D. K.; Nalage, S. R.; Khuspe, G. D.; Chougule, M. A.; Kolekar, Y. D.; Sen, S.; Patil, V. B. Synthesis of Fe₂O₃ nanoparticles for nitrogen dioxide gas sensing applications. *Ceram. Int.* **2013**, *39*, 6453.

(46) Zhang, D.; Liu, Z.; Li, C.; Tang, T.; Liu, X.; Han, S.; Lei, B.; Zhou, C. Detection of NO₂ down to ppb Levels Using Individual and Multiple In₂O₃ Nanowire Devices. *Nano Lett.* **2004**, *4*, 1919.

(47) Abbas, A. N.; Liu, B.; Chen, L.; Ma, Y.; Cong, S.; Aroonyadet, N.; Kopf, M.; Nilges, T.; Zhou, C. Black phosphorus gas sensors. *ACS Nano* **2015**, *9*, 5618.

(48) Al-Herz, M.; Simmons, M. J. H.; Wood, J. Selective hydrogenation of 1-Heptyne in a mini trickle bed reactor. *Ind. Eng. Chem. Res.* **2012**, *51*, 8815−8825.

(49) Habibpour, V.; Song, M. Y.; Wang, Z. W.; Cookson, J.; Brown, C. M.; Bishop, P. T.; Palmer, R. E. Novel powder-supported size-selected clusters for heterogeneous catalysis under realistic reaction conditions. *J. Phys. Chem. C* **2012**, *116*, 26295−26299.

(50) Cai, R. Catalytic activity of physically deposited metal clusters and their atomic structure study. PhD Thesis, University of Birmingham, 2018.